16 Dynamical Mean-Field Approximation and Cluster Methods for Correlated Electron Systems

Thomas Pruschke

Institute for Theoretical Physics, University of Göttingen, 37077 Göttingen, Germany
pruschke@theorie.physik.uni-goettingen.de

Among the various approximate methods used to study many-particle systems the simplest are mean-field theories, which map the interacting lattice problem onto an effective single-site model in an effective field. Based on the assumption that one can neglect non-local fluctuations, they allow to construct a comprehensive and thermodynamically consistent description of the system and calculate various properties, for example phase diagrams. Well-known examples for successful mean-field theories are the Weiss theory for spin models or the Bardeen-Cooper-Schrieffer theory for superconductivity. In the case of interacting electrons the proper choice of the mean-field becomes important. It turns out that a static description is no longer appropriate. Instead, a *dynamical* mean-field has to be introduced, leading to a complicated effective single-site problem, a so-called quantum impurity problem.

This chapter gives an overview of the basics of dynamical mean-field theory and the techniques used to solve the effective quantum impurity problem. Some key results for models of interacting electrons, limitations as well as extensions that systematically include non-local physics are presented.

16.1 Introduction

Strongly correlated electron systems still present a major challenge for a theoretical treatment. The simplest model describing correlation effects in solids is the one-band Hubbard model [1, 2, 3]

$$H = \sum_{i,j,\sigma} t_{ij} c^\dagger_{i\sigma} c_{j\sigma} + U \sum_i c^\dagger_{i\uparrow} c_{i\uparrow} c^\dagger_{i\downarrow} c_{i\downarrow} \,, \tag{16.1}$$

where we use the standard notation of second quantization to represent the electrons for a given lattice site $\boldsymbol{R}_i$ and spin orientation σ by annihilation (creation) operators $c^{(\dagger)}_{i\sigma}$. The first term describes a tight-binding band with tunneling amplitude for the conduction electrons t_{ij}, while the second represents the local part of the Coulomb interaction. Since for this model we assume that the conduction electrons do not have further orbital degrees of freedom, this local Coulomb interaction acts only if two electrons at the same site $\boldsymbol{R}_i$ with opposite spin are present.

The complementary nature of the two terms present in the Hubbard model (16.1) – the kinetic energy or tight-binding part is diagonal in momentum representation,

T. Pruschke: *Dynamical Mean-Field Approximation and Cluster Methods for Correlated Electron Systems*, Lect. Notes Phys. **739**, 473–503 (2008)
DOI 10.1007/978-3-540-74686-7_16

the interaction part in direct space – already indicates that it will be extremely hard to solve. One can, however, get at least for filling $\langle n \rangle = 1$ (half filling) some insight into the physics of the model by a few simple arguments: In the limit $U \to 0$ we will have a simple metal. On the other hand, for $t_{ij} \to 0$, or equivalently $U \to \infty$, the system will consist of decoupled sites with localized electrons and hence represents an insulator. We thus can expect that there exists a critical value U_{c}, where a transition from a metal to an insulator occurs. Furthermore, from second order perturbation theory around the atomic limit [4], we find that for $|t_{ij}|/U \to 0$ the Hubbard model (16.1) maps onto a Heisenberg model

$$H = \sum_{ij} J_{ij} \boldsymbol{S}_i \cdot \boldsymbol{S}_j \,, \tag{16.2}$$

where $\boldsymbol{S}_i$ represents the spin operator at site $\boldsymbol{R}_i$ and the exchange constant is given by

$$J_{ij} = 2\frac{t_{ij}^2}{U} > 0 \,. \tag{16.3}$$

Note that this immediately implies that we will have to expect that the ground state of the model at half filling will show strong antiferromagnetic correlations.

Away from half filling $\langle n \rangle \neq 1$ the situation is much less clear. There exists a theorem by Nagaoka [5], that for $U = \infty$ and one hole in the half-filled band the ground state can be ferromagnetic due to a gain in kinetic energy; to what extent this theorem applies for a thermodynamically finite doping and finite U has not been solved completely yet. The mapping to the Heisenberg model can still be performed leading to the so-called t-J model [4], which again tells us that antiferromagnetic correlations will be at least present and possibly compete with Nagaoka's mechanism for small J_{ij} or even dominate the physics if J_{ij} is large enough. This is the realm where models like the Hubbard or t-J model are thought to describe at least qualitatively the physics of the cuprate high-T_{C} superconductors [6].

The energy scales present in the model are the bandwidth W of the tight-binding band and the local Coulomb parameter U. From the discussion so far it is clear that typically we will be interested in the situation $U \approx W$ or even $U \gg W$. This means, that there is either no clear-cut separation of energy scales, or the largest energy scale in the problem is given by the two-particle interactions. Thus, standard perturbation techniques using the interaction as perturbation are usually not reliable even on a qualitative level; expansions around the atomic limit, on the other hand, are extremely cumbersome [7] and suffer from non-analyticities [8] which render calculations at low temperatures meaningless.

The knowledge on correlated electrons systems in general and the Hubbard model (16.1) in particular acquired during the past decades is therefore mainly due to the development of a variety of computational techniques, for example quantum Monte Carlo (QMC), exact diagonalization (ED), and the density-matrix renormalization group (see Parts V, VIII and IX). Since these methods – including modern developments – have been covered in great detail during this school, I will not discuss them again at this point but refer the reader to the corresponding chapters in this

book. The aspect interesting here is that basically all of them are restricted to low-dimensional systems: For ED, calculations in $D > 2$ are impossible due to the size of the Hilbert space, and in case of the DMRG the way the method is constructed restricts it basically to $D = 1$. QMC in principle can be applied to any system; however, the sign problem introduces a severe limitation to the range of applicability regarding system size, temperature or interaction strengths.

In particular the restriction to finite and usually also small systems make a reliable discussion of several aspects of the physics of correlated electron systems very hard. Typically, one expects these materials to show a rather large variety of ordered phases, ranging from different magnetic phases with and without orbital or charge ordering to superconducting phases with properties which typically cannot be accounted for in standard weak-coupling theory [9]. Moreover, metal-insulator transitions driven by correlation effects are expected [9], which are connected to a small energy scale of the electronic system. Both aspects only become visible in a macroscopically large system: For small finite lattices phase transitions into ordered states cannot appear, and an identification of such phases requires a thorough finite-size scaling, which usually is not possible. Furthermore, finite systems typically have finite-size gaps scaling with the inverse system size, which means that small low-energy scales appearing in correlated electron materials cannot be identified.

These restrictions motivate the question, if there exists a – possibly approximate – method that does not suffer from restrictions on temperature and model parameters but nevertheless works in the thermodynamic limit and thus allows for phase transitions and possibly very small low-energy scales dynamically generated due to the correlations. Such methods are the subject of this contribution.

In Sect. 16.2.1 I will motivate them on a very basic level using the concept of the mean-field theory well-known from statistical physics, and extend this concept for the Hubbard model in Sect. 16.2.2, obtaining the so-called dynamical mean-field theory (DMFT). As we will learn in Sect. 16.2.2.4, the DMFT still constitutes a non-trivial many-particle problem and I will thus briefly discuss techniques available to solve the equations of the DMFT. Following some selected results for the Hubbard model in Sect. 16.2.3 I will touch a recent development to use DMFT in material science in Sect. 16.2.4. Section 16.3 of this contribution will deal with extensions of the DMFT, which will be motivated in Sect. 16.3.1. The actual algorithms and their computational aspects will be discussed in Sects. 16.3.2 and 16.3.3. Some selected results for the Hubbard model in Sect. 16.3.4 will finish this chapter.

16.2 Mean-Field Theory for Correlated Electron Systems

16.2.1 Classical Mean-Field Theory for the Heisenberg Model

In the introduction to the Hubbard model we already encountered the Heisenberg model (16.2) as low-energy limit for $U \to \infty$. Regarding its solvability, this model shares some more features with the Hubbard model in that it poses a computational rather hard problem in $D \geq 2$. However, there exists a very simple approximate

theory which nevertheless describes the properties of the Heisenberg model at least qualitatively correct, the Weiss mean-field theory [10]. As we all learned in the course on statistical physics, the basic idea of this approach is the approximate replacement

$$\boldsymbol{S}_i \cdot \boldsymbol{S}_j \approx \boldsymbol{S}_i \cdot \langle \boldsymbol{S}_j \rangle_{\mathrm{MFT}} + \langle \boldsymbol{S}_i \rangle_{\mathrm{MFT}} \cdot \boldsymbol{S}_j \tag{16.4}$$

$$H \approx \sum_i H^{(i)}_{\mathrm{MFT}} = 2 \sum_{ij} J_{ij} \boldsymbol{S}_i \cdot \langle \boldsymbol{S}_j \rangle_{\mathrm{MFT}} \tag{16.5}$$

where $\langle \ldots \rangle_{\mathrm{MFT}}$ stands for the thermodynamic average with respect to the mean-field Hamiltonian (16.5) and we dropped a for the present discussion unimportant term $\langle \boldsymbol{S}_i \rangle_{\mathrm{MFT}} \cdot \langle \boldsymbol{S}_j \rangle_{\mathrm{MFT}}$. If we define an effective magnetic field or Weiss field according to

$$\boldsymbol{B}_{i,\mathrm{MF}} := 2 \sum_{j \neq i} J_{ij} \langle \boldsymbol{S}_j \rangle_{\mathrm{MF}} \ , \tag{16.6}$$

we may write

$$H^{(i)}_{\mathrm{MF}} = \boldsymbol{S}_i \cdot \boldsymbol{B}_{i,\mathrm{MF}} \ . \tag{16.7}$$

This replacement is visualized in Fig. 16.1. The form (16.7) also explains the name assigned to the theory: The Hamiltonian (16.2) is approximated by a single spin in an effective magnetic field, the mean-field, given by the average over the surrounding spins. Note that this treatment does not make any reference to the system size, i.e. it is also valid in the thermodynamic limit.

The fact, that the mean-field $\boldsymbol{B}_{i,\mathrm{MF}}$ is determined by $\langle \boldsymbol{S}_j \rangle_{\mathrm{MFT}}$ immediately leads to a self-consistency condition for the latter

$$\langle \boldsymbol{S}_i \rangle_{\mathrm{MFT}} = \mathcal{F} \left[\langle \boldsymbol{S}_j \rangle_{\mathrm{MFT}} \right] \ . \tag{16.8}$$

The precise form of the functional will in general depend on the detailed structure of the Hamiltonian (16.2). For a simple cubic lattice and nearest-neighbor exchange

$$J_{ij} = \begin{cases} J & \text{for } i,j \text{ nearest neighbors} \\ 0 & \text{otherwise} \end{cases} \tag{16.9}$$

one finds the well-known result

$$\langle S^z_i \rangle_{\mathrm{MFT}} = -\frac{1}{2} \tanh \left(\frac{4DJ \langle S^z_j \rangle_{\mathrm{MFT}}}{k_{\mathrm{B}} T} \right) \ , \tag{16.10}$$

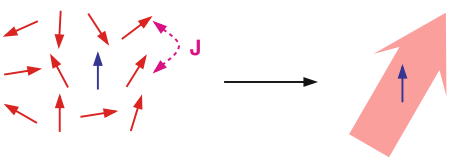

Fig. 16.1. Sketch for the mean-field theory of the Heisenberg model

where we put the quantization axis into the z direction and assumed the same value $\langle S_j^z \rangle_{\text{MFT}}$ for all $2D$ nearest neighbors. For $k_{\text{B}}T < |J^*|$, where $J^* := 2DJ$, this equation has a solution $|\langle S_i^z \rangle_{\text{MFT}}| \neq 0$, i.e. the system undergoes a phase transition to an ordered state (antiferromagnetic for $J > 0$ and ferromagnetic for $J < 0$).

As we know, this mean-field treatment yields the qualitatively correct phase diagram for the Heisenberg model in $D = 3$, but fails in dimensions $D \leq 2$ and close to the phase transition for $D = 3$. The reason is that one has neglected the fluctuations $\delta \boldsymbol{S}_i = \boldsymbol{S}_i - \langle \boldsymbol{S}_i \rangle$ of the neighboring spins. Under what conditions does that approximation become exact? The answer is given in [10]: The mean-field approximation becomes exact in the formal limit $D \to \infty$, provided on keeps $J^* = 2DJ$ constant. In this limit, each spin has $2D \to \infty$ nearest neighbors (for a simple cubic lattice). Assuming ergodicity of the system, one finds that the phase space average realized by the sum over nearest neighbors becomes equal to the ensemble average, i.e.

$$\frac{1}{2D} \sum_{j \neq i} \boldsymbol{S}_j \overset{D \to \infty}{=} \frac{1}{2D} \sum_{j \neq i} \langle \boldsymbol{S}_j \rangle + \mathcal{O}(\frac{1}{D}) \; . \tag{16.11}$$

The requirement $J^* =$const. finally is necessary, because otherwise the energy density $\langle H \rangle / N$ would either be zero or infinity, and the resulting model would be trivial.

For the Heisenberg model (16.2) one can even show that $D > 3$ is already sufficient to make the mean-field treatment exact, which explains why this approximation can yield a rather accurate description for magnets in $D = 3$.

Obviously, the above argument based on the limit $D = \infty$ is rather general and can be applied to other models to define a proper mean-field theory. For example, applied to disorder models, one obtains the coherent potential approximation (CPA), where the disorder is replaced by a coherent local scattering potential, which has to be determined self-consistently via the disorder average. A more detailed discussion of the capabilities and shortcomings of this mean-field theory is given in Chap. 17. Here, we want to use the limit $D \to \infty$ to construct a mean-field theory for models like the Hubbard model (16.1).

16.2.2 The Dynamical Mean-Field Theory

16.2.2.1 A First Attempt

Guided by the previous section, the most obvious possibility to construct something like a mean-field theory for the Hubbard model (16.1) is to approximate the two-particle interaction term as

$$c_{i\uparrow}^\dagger c_{i\uparrow} c_{i\downarrow}^\dagger c_{i\downarrow} \to c_{i\uparrow}^\dagger c_{i\uparrow} \langle c_{i\downarrow}^\dagger c_{i\downarrow} \rangle + \langle c_{i\uparrow}^\dagger c_{i\uparrow} \rangle c_{i\downarrow}^\dagger c_{i\downarrow} \; . \tag{16.12}$$

This approximation, which is also known as Hartree approximation, is discussed extensively in standard books on many particle theory (for example [11]). Without going into the details, one can immediately state some serious defects for half filling $\langle n \rangle = 1$:

– It leads to a metallic solution for arbitrarily large U, in contradiction to the expectations based on fundamental arguments.
– One does find an antiferromagnetically ordered phase, but for large U the Néel temperature $T_{\mathrm{N}} \rightarrow$const. instead of the expectation $T_{\mathrm{N}} \propto 1/U$ based on the mapping (16.3) to the antiferromagnetic Heisenberg model.

What goes wrong here? The answer is quite simple: The Hartree factorization neglects *local* charge fluctuations

$$\delta n_{i\sigma} = c^\dagger_{i\sigma} c_{i_\sigma} - \langle c^\dagger_{i\sigma} c_{i_\sigma} \rangle \tag{16.13}$$

which however are of order one. Thus, an argument rendering this approximation exact in a nontrivial limit is missing here.

16.2.2.2 The Limit $D \rightarrow \infty$

As we have observed in Sect. 16.2.1, the proper way to set up a mean-field theory is to consider the limit $D \rightarrow \infty$. Again, this limit has to be introduced such that the energy density $\langle H \rangle / N$ remains finite. As far as the interaction term in (16.1) is concerned, no problem arises, because it is purely local and thus does not care about dimensionality. The critical part is obviously the kinetic energy

$$\frac{1}{N}\langle H_{\mathrm{kin}} \rangle = \frac{1}{N} \sum_{i,j} \sum_{\sigma} t_{ij} \langle c^\dagger_{i\sigma} c_{j\sigma} \rangle \ . \tag{16.14}$$

To keep the notation simple, I will concentrate on a simple cubic lattice with nearest-neighbor hopping

$$t_{ij} = \begin{cases} -t & \text{for } \boldsymbol{R}_i \text{ and } \boldsymbol{R}_j \text{ nearest neighbors} \\ 0 & \text{otherwise} \end{cases} \tag{16.15}$$

in the following. Starting at a site $\boldsymbol{R}_i$, one has to apply H_{kin} to move an electron to or from site $\boldsymbol{R}_j$ in the nearest-neighbor shell, i.e. $\langle c^\dagger_{i\sigma} c_{j\sigma} \rangle \propto t$ and consequently

$$\frac{1}{N}\langle H_{\mathrm{kin}} \rangle = \frac{1}{N} \sum_{i,j} \sum_{\sigma} t_{ij} \langle c^\dagger_{i\sigma} c_{j\sigma} \rangle \propto -2Dt^2 \ , \tag{16.16}$$

where the factor $2D$ arises because we have to sum over the $2D$ nearest neighbors [12]. Thus, in order to obtain a finite result in the limit $D \rightarrow \infty$, it has to be performed such that $Dt^2 = t^* =$const. or $t = t^*/\sqrt{D}$ [12].

What are the consequences of this scaling? To find an answer to this question, let us consider the quantity directly related to $\langle c^\dagger_{i\sigma} c_{j\sigma} \rangle$, namely the single-particle Green function [11]

$$G_{\boldsymbol{k}\sigma}(z) = \frac{1}{z + \mu - \epsilon_{\boldsymbol{k}} - \Sigma_{\boldsymbol{k}\sigma}(z)} \ , \tag{16.17}$$

where the kinetic term enters as dispersion $\epsilon_{\boldsymbol{k}}$, obtained from the Fourier transform of t_{ij}, and the two-particle interaction leads to the self-energy $\Sigma_{\boldsymbol{k}\sigma}(z)$, which can, for example, be obtained from a perturbation series using Feynman diagrams [11]. For the following argument it is useful, to discuss the perturbation expansion in real space, i.e. we study now $\Sigma_{ij,\sigma}(z)$. If we represent the Green function $G^{(0)}_{ij,\sigma}(z)$ for $U = 0$ by a (directed) full line and the two-particle interaction U by a dashed line, the first few terms of the Feynman perturbation series read

$$\Sigma_{ij,\sigma}(z) = \quad \delta_{ij} + \quad + \ldots \; . \tag{16.18}$$

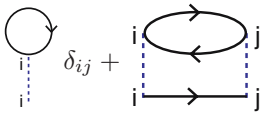

The first, purely local term, evaluates to $U\langle n_{i\bar{\sigma}}\rangle$, i.e. it is precisely the Hartree approximation which we found not sufficient to reproduce at least the fundamental expectations. Let us now turn to the second term. To discuss it further, we need the important property $G^{(0)}_{ij,\sigma}(z) \propto t^{d(i,j)}$, where $d(i,j)$ is the "taxi-cab metric", i.e. the smallest number of steps to go from site $\boldsymbol{R}_i$ to site $\boldsymbol{R}_j$. Inserting the scaling $t = t^*/\sqrt{D}$, we find

$$G^{(0)}_{ij,\sigma}(z) \propto \left(\frac{1}{\sqrt{D}}\right)^{d(i,j)} \; . \tag{16.19}$$

When we insert this scaling property into the second-order term in the expansion (16.2.2.2), we obtain for j being a nearest neighbor of i

$$\Sigma_{ij,\sigma}(z) - U\langle n_{i\bar{\sigma}}\rangle\delta_{ij} = \quad + \ldots \propto \left(\frac{1}{\sqrt{D}^3}\right)^{d(i,j)} \propto \frac{1}{\sqrt{D}^3} \; . \tag{16.20}$$

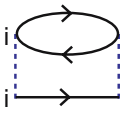

A closer inspection [12] yields an additional factor D on the right-hand side of the equation, and we finally arrive at the scaling behavior

$$\Sigma_{ij,\sigma}(z) - U\langle n_{i\bar{\sigma}}\rangle\delta_{ij} \propto \frac{1}{\sqrt{D}} \overset{D\to\infty}{\to} 0 \tag{16.21}$$

for the non-local part of the one-particle self-energy. Note that the local contributions $\Sigma_{ii,\sigma}(z)$ stay finite, i.e.

$$\lim_{D\to\infty} \Sigma_{ij,\sigma}(z) = \Sigma_\sigma(z)\delta_{ij} \; , \tag{16.22}$$

which in momentum space translates into a $\boldsymbol{k}$-independent self-energy and hence

$$G_{\boldsymbol{k}\sigma}(z) = \frac{1}{z + \mu - \epsilon_{\boldsymbol{k}} - \Sigma_\sigma(z)} \; . \tag{16.23}$$

The finding that in the limit $D \to \infty$ renormalizations due to local two-particle interactions become purely local, is rather interesting and helpful in its own right. For example, one can use it to set up a perturbation theory which is, due to the missing spatial degrees of freedom, much more easy to handle. Within this framework, the Hubbard model and related models were studied by several groups studying low-energy dynamics and transport properties [13, 14, 15] or the phase diagram at weak coupling $U \to 0$ [16, 17, 18]. There is, however, an additional way one can make use of the locality of the self-energy, which directly leads to the theory nowadays called dynamical mean-field theory (DMFT).

16.2.2.3 Mean-Field Theory for the Hubbard Model

The fundamental observation underlying the DMFT, namely that one can use the locality of the self-energy to map the lattice model onto an effective impurity problem, was first made by Brandt and Mielsch [19]. For the actual derivation of the DMFT equations for the Hubbard model one can use several different techniques. I will here present the one based on a comparison of perturbation expansions [20]. A more rigorous derivation can for example be found in the review by Georges et al. [21]. Let us begin by calculating the local Green function $G_{ii,\sigma}(z)$, which can be obtained from $G_{\boldsymbol{k}\sigma}(z)$ by summing over all $\boldsymbol{k}$, i.e.

$$G_{ii,\sigma}(z) = \frac{1}{N}\sum_{\boldsymbol{k}} \frac{1}{z+\mu-\epsilon_{\boldsymbol{k}}-\Sigma_\sigma(z)} \; . \tag{16.24}$$

Since $\boldsymbol{k}$ appears only in the dispersion, we can rewrite the $\boldsymbol{k}$-sum as integral over the density of states (DOS) of the model with $U = 0$

$$\rho^{(0)}(\epsilon) = \frac{1}{N}\sum_{\boldsymbol{k}} \delta(\epsilon - \epsilon_{\boldsymbol{k}}) \tag{16.25}$$

as

$$G_{ii,\sigma}(z) = \int \mathrm{d}\epsilon \frac{\rho^{(0)}(\epsilon)}{z+\mu-\epsilon-\Sigma_\sigma(z)} = G^{(0)}_{ii}(z+\mu-\Sigma_\sigma(z)) \; , \tag{16.26}$$

where

$$G^{(0)}_{ii}(\zeta) = \int \mathrm{d}\epsilon \frac{\rho^{(0)}(\epsilon)}{\zeta-\epsilon} \tag{16.27}$$

is the local Green function for $U = 0$. Note that due to the analytic properties of $\Sigma_\sigma(z)$ the relation $\mathrm{sign}\{\mathrm{Im}\,[z+\mu-\Sigma_\sigma(z)]\} = \mathrm{sign}\,\mathrm{Im}\,z$ always holds.

Now we can make use of well-known properties of quantities like $G^{(0)}_{ii}(z)$ which can be represented as Hilbert transform of a positive semi-definite function like the DOS $\rho^{(0)}(\epsilon)$ (see for example [11]), namely they can quite generally be written as

$$G^{(0)}_{ii}(\zeta) = \frac{1}{\zeta - \widetilde{\Delta}(\zeta)} \; , \tag{16.28}$$

where $\widetilde{\Delta}(\zeta)$ is completely determined by $\rho^{(0)}(\epsilon)$. If we define $\mathcal{G}_\sigma(z)^{-1} := z + \mu - \Delta_\sigma(z)$, where $\Delta_\sigma(z) := \widetilde{\Delta}(z + \mu - \Sigma_\sigma(z))$, we can write the Green function for $U > 0$ as

$$G_{ii,\sigma}(\zeta) = \frac{1}{z + \mu - \Delta_\sigma(z) - \Sigma_\sigma(z)} = \frac{1}{\mathcal{G}_\sigma(z)^{-1} - \Sigma_\sigma(z)} \,. \tag{16.29}$$

Let us now assume that we switch off U at site $\boldsymbol{R}_i$ only. Then $\mathcal{G}_\sigma(z)$ can be viewed as non-interacting Green function of an impurity model with a perturbation series

$\Sigma_\sigma(z) =$ 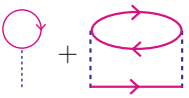 $+ \ldots$ (16.30)

for the self-energy. The full line now represents $\mathcal{G}_\sigma(z)$, but the dashed line visualizes still the same two-particle interaction as in (16.2.2.3). Looking into the literature, for example into the book by Hewson [22], one realizes that this is precisely the perturbation expansion for the so-called single impurity Anderson model (SIAM) [23]

$$H = \sum_{\boldsymbol{k}\sigma} \varepsilon_{\boldsymbol{k}} \alpha^\dagger_{\boldsymbol{k}\sigma} \alpha_{\boldsymbol{k}\sigma} + \varepsilon_f \sum_\sigma c^\dagger_\sigma c_\sigma + U c^\dagger_\uparrow c_\uparrow c^\dagger_\downarrow c_\downarrow + \frac{1}{\sqrt{N}} \sum_{\boldsymbol{k}\sigma} \left(\alpha^\dagger_{\boldsymbol{k}\sigma} c_\sigma + \text{H.c.} \right) , \tag{16.31}$$

which has been studied extensively in the context of moment formation in solids.

Obviously, the quantity $\mathcal{G}_\sigma(z)$ – or equivalently $\Delta_\sigma(z)$ – takes the role of the Weiss field in the MFT for the Heisenberg model. However, in contrast to the MFT for the Heisenberg model, where we ended up with an effective Hamiltonian of a single spin in a static field, we now have an effective local problem which is coupled to a dynamical field, hence the name DMFT. Instead of Weiss field, $\mathcal{G}_\sigma(z)$ or $\Delta_\sigma(z)$ are called effective medium in the context of the DMFT.

The missing link to complete the mean-field equations is the self-consistency condition which relates the Weiss field $\mathcal{G}_\sigma(z)$ with the solution of the effective impurity problem. This reads

$$G_{ii,\sigma}(z) = \int \mathrm{d}\epsilon \frac{\rho^{(0)}(\epsilon)}{z + \mu - \epsilon - \Sigma_\sigma(z)} \stackrel{!}{=} G^{\text{SIAM}}_\sigma(z) \,. \tag{16.32}$$

Thus, $\Sigma_\sigma(z)$ has to be chosen such that the local Green function of the Hubbard model is identical to the Green function of a fictitious SIAM with non-interacting Green function

$$\mathcal{G}_\sigma(z) = \frac{1}{G_{ii,\sigma}(z)^{-1} + \Sigma_\sigma(z)} \,. \tag{16.33}$$

The resulting flow-chart for the iterative procedure to solve the Hubbard model

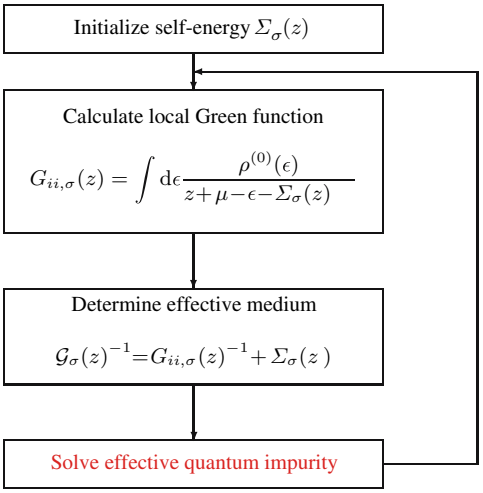

Fig. 16.2. The self-consistency loop for the DMFT for the Hubbard model

with the DMFT is shown in Fig. 16.2. The only unknown in it is the box at the bottom saying "solve effective quantum impurity problem". What the notion quantum impurity stands for and how the SIAM can be solved will be discussed next.

16.2.2.4 DMFT as Quantum Impurity Problem

Up to now all considerations have been purely analytical. Since this is a book on computational aspects in many-body systems, one may wonder how this theory fits into this field. The simple answer lies in the solution of the SIAM necessary to complete the DMFT loop. Although the Hamiltonian (16.31) of the SIAM looks comparatively simple, it is already an extremely challenging model. It has been set up in the early 1960's, but a reliable solution for both thermodynamic and dynamic quantities at arbitrary model parameters and temperature became possible only in the late 1980's. It belongs to a class of models nowadays called quantum-impurity models, where a small set of interacting quantum degrees of freedom are coupled to a continuum of non-interacting quantum states. The physical properties of these models comprise the well-known Kondo effect [22], quantum phase transitions and non-Fermi liquid behavior. The actual difficulty in solving these models is that they typically have a ground state that in the thermodynamical limit is orthogonal to the one of the possible reference systems – e.g. $U = 0$ or $V_{\boldsymbol{k}} = 0$ for the SIAM – and thus cannot be treated properly with perturbation expansions. A characteristic signature of this non-orthogonality is the appearance of an exponentially small energy scale. Both aspects together make it extremely hard to solve the models even numerically, because any representation by a finite system makes it impossible to resolve such energy scales.

Besides the numerical renormalization group discussed in the next paragraph, one of the first computational techniques used to solve quantum impurity problems

for finite temperatures was quantum Monte Carlo based on the Hirsch-Fye algorithm [21, 24]. This algorithm and its application to e.g. Hubbard model has already been discussed extensively in Chap. 10. For these models, the short-ranged interaction and hopping allow for a substantial reduction of the computational effort and a rather efficient code. For quantum impurity problems, however, the orthogonality catastrophe mentioned above leads to long-ranged correlations in imaginary time. Consequently, when we denote with L the number of time slices in the simulation, the code scales with L^3 (instead of $L \ln L$ for lattice models [25]). Thus, although the algorithm does not show a sign problem for quantum impurity problems, the computational effort increases very strongly with decreasing temperature and also increasing local interaction. As a result, the quantum Monte Carlo based on the Hirsch-Fye algorithm is severely limited in the temperatures and interaction parameters accessible. For those interested, a rather extensive discussion of the algorithm and its application to the DMFT can be found in the reviews by Georges et al. and Maier et al. [21, 24]. Note that with quantum Monte Carlo one is generically restricted to finite temperature, although within the projector quantum Monte Carlo the ground state properties can be accessed in some cases, too [26].

A rather clever method to handle quantum-impurity systems comprising such a huge range of energy scales was invented by Wilson in the early 1970's [27], namely the numerical renormalization group (NRG). In this approach, the continuum of states is mapped onto a discrete set, however with exponentially decreasing energy scales. This trick allows to solve models like the SIAM for arbitrary model parameters and temperatures. A detailed account of this method is beyond the scope of this contribution but can be found in a recent review by Bulla et al. [28]. Here, the interesting aspect is the actual implementation. One introduces a discretization parameter $\Lambda > 1$ and divides the energy axis into intervals $[\Lambda^{-(n+1)}, \Lambda^{-n}]$, $n = 0, 1, \ldots$, for both positive and negative energies. After some manipulations [22, 28, 29, 30] one arrives at a representation

$$H \approx H_{\text{imp}} + \sum_{n=0}^{\infty} \sum_{\sigma} \left(\varepsilon_n \alpha^{\dagger}_{n\sigma} \alpha_{n\sigma} + t_n \alpha^{\dagger}_{n-1\sigma} \alpha_{n\sigma} + \text{H.c.} \right) , \tag{16.34}$$

where H_{imp} is the local part of the quantum impurity Hamiltonian. To keep the notation short, I represented the impurity degrees of freedom by the operators $\alpha^{(\dagger)}_{-1,\sigma}$. The quantities ε_n and t_n have the property, that they behave like $\varepsilon_n \propto \Lambda^{-n/2}$ and $t_n \propto \Lambda^{-n/2}$ for large n. The calculation now proceeds as follows: Starting from the impurity degrees of freedom ($n = -1$) with the Hamiltonian $H_{-1} \equiv H_{\text{imp}}$, one successively adds site after site of the semi-infinite chain, generating a sequence of Hamiltonians

$$\begin{aligned} H_{N+1} = \sqrt{\Lambda} H_N + \sum_{\sigma} \Big(& \sqrt{\Lambda}^{N+1} \varepsilon_{N+1} \alpha^{\dagger}_{N+1,\sigma} \alpha_{N+1,\sigma} \\ & + \sqrt{\Lambda}^{N+1} t_{N+1} \alpha^{\dagger}_{n\sigma} \alpha_{n\sigma} + \text{H.c.} \Big) . \end{aligned} \tag{16.35}$$

The factors Λ in the mapping ensure that at each step N the lowest energy eigenvalues are always of order one. Since for the chain parameters $\Lambda^{(N+1)/2} t_{N+1} \to 1$ holds, the high energy states of the Hamiltonian at step N will not significantly contribute to the low-energy states at step $N+1$ and one discards them. This truncation restricts the size of the Hilbert space at each step sufficiently that the usual exponential growth is suppressed and one can actually repeat the procedure up to almost arbitrarily large chains.

At each step N, one then has to diagonalize H_N, generating all eigenvalues and eigenvectors. The eigenvectors are needed to calculate matrix elements for the next step by a unitary transformation of the matrix elements from the previous step. Since this involves two matrix multiplications, the numerical effort (together with the diagonalization) scales with the third power of the dimension of the Hilbert space. Invoking symmetries of the system, like e.g. charge and spin conservation, one can reduce the Hamilton matrix at each step to a block structure. This block structure on the one hand allows for an efficient parallelization and use of SMP machines (for example with OpenMP). On the other hand, the size of the individual blocks is much smaller than the actual size of the Hilbert space. For example, with 1000 states kept in the truncation one has a dimension of the order of 200 for the largest subblock. The use of the block structure thus considerably reduces the computational effort necessary at each step.

Moreover, one can identify each chain length N with a temperature or energy scale $\Lambda^{-N/2}$ and can thus approach arbitrarily low temperatures and energies. With presently available workstations the computational effort of solving the effective impurity model for DMFT calculations at $T = 0$ then reduces to a few minutes using on the order of $10 \ldots 100$ MB of memory.

Unfortunately, an extension of Wilson's NRG to more complex quantum impurity models including e.g. orbital degrees of freedom or multi-impurity systems (needed for example for the solution of cluster mean-field theories, see Sect. 16.3) is not possible beyond four impurity degrees of freedom (where the consumption of computer resources increases to order of days computation time with $\sim 20 - 30$ GB memory usage), because the step "construct Hamilton matrix of step $N+1$ from Hamilton matrix of step N" increases the size again exponentially with respect to the number of impurity degrees of freedom. For a compensation, one has to increase the number of truncated states in each step appropriately. However, this procedure breaks down when one starts to truncate states that contribute significantly to the low-energy properties of the Hamiltonian at step $N+1$. In this situation, one is left with quantum Monte Carlo algorithms as only possible solver at $T > 0$. At $T = 0$, there exists presently not yet a reliable tool to solve quantum impurity models with substantially more that two impurity degrees of freedom (spin degeneracy). First attempts to use the density matrix renormalization group method to solve quantum impurity problems can for example be found in [31, 32, 33].

16.2.3 DMFT Results for the Hubbard Model

In the following sections selected results for the Hubbard model within the DMFT will be discussed. I restrict the presentation to the case of a particle-hole symmetric

non-interacting system, i.e. the simple-cubic lattice with nearest-neighbor hopping according to (16.15). More general situations including next nearest-neighbor hopping have also been studied and results can for example be found in [21, 34]. Moreover, the DMFT also allows for a consistent calculation of two-particle properties like susceptibilities and also transport quantities. A detailed discussion of the aspects of these calculations go well beyond the scope of this article and the interested reader is referred to the extensive literature on these subjects [21, 24, 35].

16.2.3.1 General Structures of the Green Function in DMFT

The fundamental quantity we calculate in the DMFT is the local single-particle Green function $G_{ii,\sigma}(z)$. Its imaginary part $N_\sigma(\omega) := -\operatorname{Im} G_{ii,\sigma}(\omega + i0^+)/\pi$ is called DOS of the interacting system. The generic result for this quantity for a typical value of $U = \mathcal{O}(W)$ at $T = 0$, where W is the bandwidth of the dispersion $\epsilon_{\boldsymbol{k}}$, is shown in Fig. 16.3 [21, 35]. One can identify three characteristic structures: Two broad peaks below and above the Fermi energy $\omega = 0$, which describe the incoherent charge excitations. They are separated by the energy U and referred to as lower Hubbard band (LHB) and upper Hubbard band (UHB), respectively. In addition a rather sharp resonance exists at the Fermi energy, which is a result of coherent quasiparticles in the sense of Landau's Fermi liquid theory.

This interpretation becomes more apparent when one looks at the single-particle self-energy, shown as inset to Fig. 16.3. The region close to the Fermi energy is characterized by a behavior $\operatorname{Re} \Sigma_\sigma(\omega + i0^+) \propto \omega$ and $\operatorname{Im} \Sigma_\sigma(\omega + i0^+) \propto \omega^2$. Both

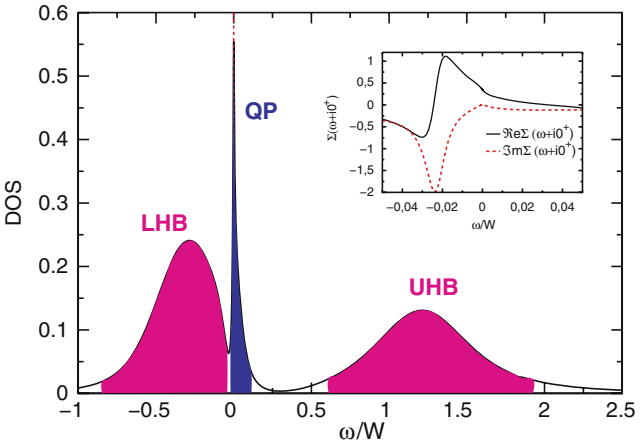

Fig. 16.3. Generic DMFT result for the DOS of the Hubbard model at $T = 0$. Model parameters are $U/W = 1.5$ and $\langle n \rangle = 0.97$. W denotes the bandwidth of the dispersion $\epsilon_{\boldsymbol{k}}$. The inset shows the corresponding self-energy $\Sigma_\sigma(\omega + i0^+)$ in the region about the Fermi energy. One nicely sees the parabolic maximum in the imaginary part and the linear real part as $\omega \to 0$

are features characteristic for a Fermi liquid. The slope of the real part determines the quasiparticle renormalization factor or effective mass of the quasiparticles.

16.2.3.2 The Mott-Hubbard Metal-Insulator Transition

One particular feature we expect for the Hubbard model is the occurrence of a metal-insulator transition (MIT) in the half-filled case $\langle n \rangle = 1$. As already mentioned, this particular property can serve as a test for the quality of the approximation used to study the model. That the expected MIT indeed appears in the DMFT has first been noticed by Jarrell [20] and was subsequently studied in great detail [21]. The MIT shows up in the DOS as vanishing of the quasiparticle peak with increasing U. An example for this behavior can be seen in Fig. 16.4. The full curve is the result of a calculation with a value of $U < W$, the dashed obtained with $U > 1.5\,W \approx U_c$. For the latter, the quasiparticle peak at $\omega = 0$ has vanished, i.e. we have $N(\omega = 0) = 0$. Since the DOS at the Fermi level determines all properties of a Fermi system, in particular the transport, we can conclude from this result that for $U > U_c$ the conductivity will be zero, hence the system is an insulator. One can now perform a series of calculations for different values of U and temperatures T to obtain the phase diagram for this MIT (see e.g. [36] and references therein). The result is shown in Fig. 16.5. As an unexpected feature of this MIT one finds that there exists a hysteresis region, i.e. starting from a metal and increasing U leads to a different $U_{c,2}$ as starting from the insulator at large U and decreasing U. The coexistence region terminates in a second-order critical end point, which has the properties of the liquid-gas transition [37, 38]. At $T = 0$, the transition is also second order and characterized by a continuously vanishing Drude weight in the optical conductivity [21], or equivalently a continuously vanishing quasiparticle renormalization factor [39]. Interestingly, the actual critical line falls almost onto the

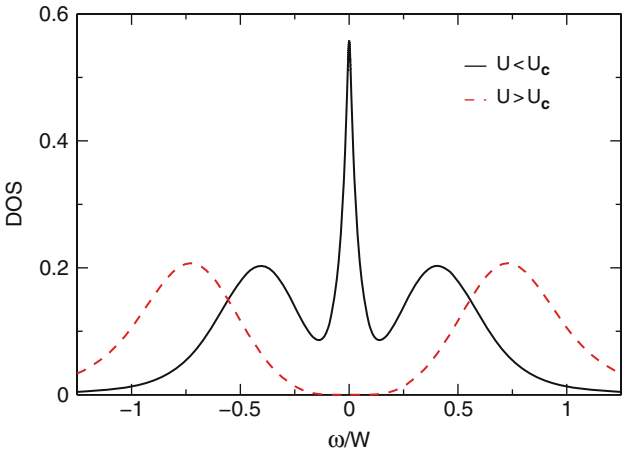

Fig. 16.4. Variation of DOS across the MIT

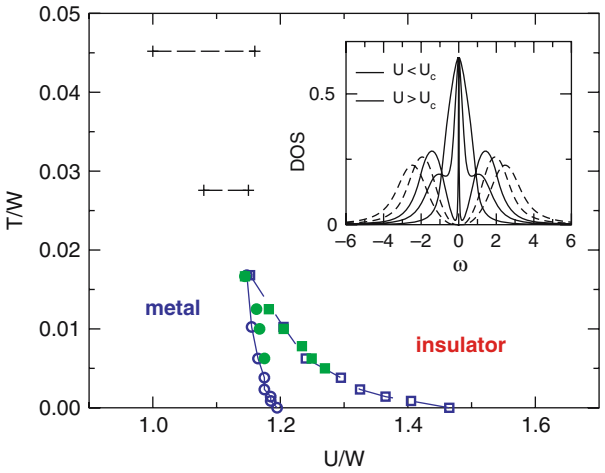

Fig. 16.5. Paramagnetic phase diagram for the Hubbard model at half filling. The transition between metal and insulator shows a hysteresis denoted by the *two critical lines*. The inset shows the behavior of the DOS as U increases. Figure taken from [36]

upper transition [40]. Finally, for temperatures larger than the upper critical point the MIT turns into a crossover.

16.2.3.3 Magnetic Properties

Up to now we have discussed the paramagnetic phase of the Hubbard model. What about the magnetic properties? Does the DMFT in particular cure the failure of the Hartree approximation, where T_{N} became constant when $U \to \infty$?

Investigations of magnetic properties can be done in two ways. First, one can calculate the static magnetic susceptibility and search for its divergence. This will give besides the transition temperature also the proper wave vector of the magnetic order [21, 41]. For the NRG another method is better suited and yields furthermore also information about the single-particle properties and hence transport properties in the antiferromagnetic phase [21, 34]: One starts the calculation with a small symmetry breaking magnetic field, which will be switched off after the first DMFT iteration. As result, the system will converge either to a paramagnetic state or a state with finite polarization. The apparent disadvantage is, that only certain commensurate magnetic structures can be studied, such as the ferromagnet or the Néel antiferromagnet.

For half filling, the result of such a calculation for the Néel structure at $T = 0$ is shown in Fig. 16.6. Quite generally, we expect a stable antiferromagnetic phase at arbitrarily small values of U with an exponentially small Néel temperature [11, 16]. Indeed we find that the Néel antiferromagnet is the stable solution for all values of U at $T = 0$ [42].

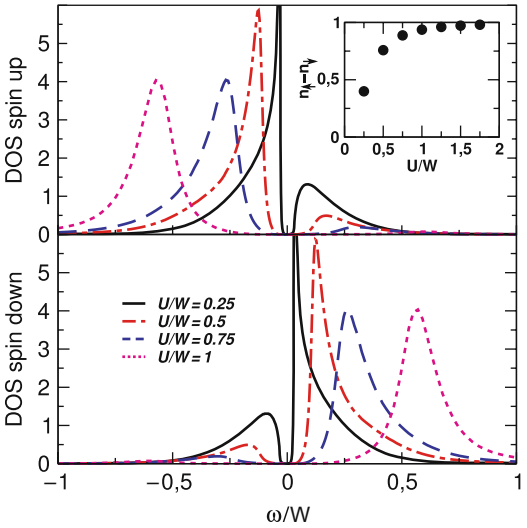

Fig. 16.6. DOS for spin up and spin down in the antiferromagnetic phase at half filling and $T = 0$. The inset shows the magnetization as function of U

The next question concerns the magnetic phase diagram, in particular the dependence of the Néel temperature T_N on U. To this end one has to perform a rather large number of DMFT calculations systematically varying T and U. The result of such a survey are the circles denoting the DMFT values for $T_\mathrm{N}(U)$ in the phase diagram in Fig. 16.7. The dotted line is a fit that for small U behaves $\propto \exp(-\alpha/U)$, predicted by weak-coupling theory, while for large U a decay like $1/U$ is reached. Thus, the DMFT indeed reproduces the correct U dependence in both limits $U \to 0$ and $U \to \infty$.

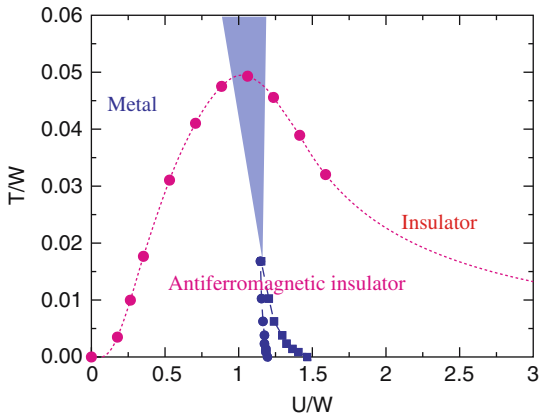

Fig. 16.7. Phase diagram for the Néel state at half filling. In addition the paramagnetic MIT phase lines are included

Another observation is that the phase diagram is completely dominated by the Néel phase. It even encompasses the MIT phase, whose phase lines are given by the squares in Fig. 16.7. Note, that the Néel phase is an insulator, too. Thus, there is the obviously interesting question if an additional transition occurs within the antiferromagnetic insulator from what is called Slater insulator, driven by bandstructure effects, and Mott-Hubbard insulator, driven by correlation effects. Up to now, no hard evidence for such a transition could be found [34, 43].

Last, but not least, one may wonder how the magnetic phase diagram develops away from half filling. Here, two interesting conjectures are known. Weak coupling theory predicts, that for small U the Néel state remains stable up to a certain filling $\langle n_c \rangle < 1$, but shows phase separation [18]. In the limit $U \to \infty$, on the other hand, one expects a ferromagnetic phase to appear, which is driven by kinetic energy gain instead of an effective exchange interaction [5]. Here, the full power of the NRG as solver for the quantum impurity problem can be seen. There are no restrictions regarding the value of U or the temperature T. Consequently, one can scan the whole phase space of the Hubbard model to obtain the U-δ phase diagram at $T = 0$ shown in Fig. 16.8. The quantity $\delta = 1 - \langle n \rangle$ denotes the doping and the vertical axis has been rescaled according to $U/(W + U)$ in order to show the results for the whole interval $U \in [0, \infty)$. One indeed finds an extended region of antiferromagnetism (AFM) for finite doping, which in addition shows phase separation (PS) for values $U < W$. For larger U, the actual magnetic structure could not be resolved yet [42]. At very large U the antiferromagnet is replaced by an extended island of Nagaoka type ferromagnetism (FM) extending out to $\approx 30\%$ doping [42]. These examples show that the DMFT is indeed capable of reproducing at least qualitatively the rather

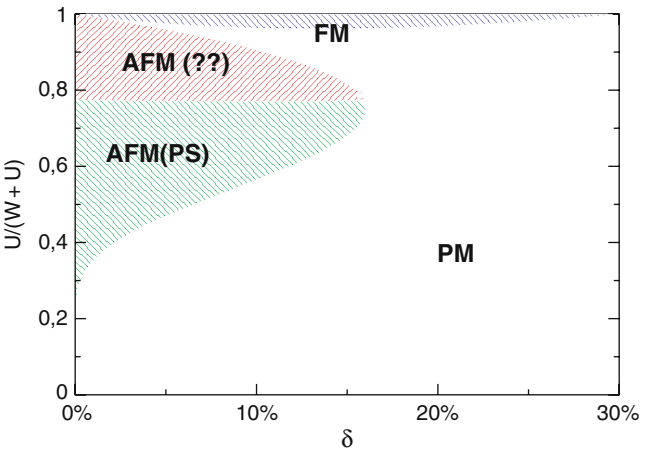

Fig. 16.8. Magnetic phase diagram of the Hubbard model for $T = 0$. The vertical axis has been rescaled as $U/(W+U)$ to encompass the whole interval $[0, \infty)$. The abbreviations mean paramagnetic metal (PM), antiferromagnet (AFM), phase separation (PS) and ferromagnet (FM). $\delta = 1 - \langle n \rangle$ denotes the doping

complex physical properties of the Hubbard model (16.1). Moreover, the values for transition temperatures obtained are strongly reduced as compared to a Stoner or Hartree approximation [11], thus illuminating the importance of local dynamical fluctuations due to the two-particle interaction respected by the DMFT.

16.2.4 Further Application: Combining First Principles with DMFT

The finding, that the DMFT for the Hubbard model, besides properly reproducing all expected features at least qualitatively, also leads to a variety of non-trivial novel aspects of the physics of this comparatively simple model [21, 35], rather early triggered the expectation, that this theory can also be a reasonable ansatz to study real 3D materials. This idea was further supported by several experimental results on transition metal compound suggesting that the metallic state can be described as a Fermi liquid with effective masses larger than the ones predicted by bandstructure theory [9]. Moreover, with increasing resolution of photoemission experiments, structures could be resolved that very much looked like the ubiquitous lower Hubbard band and quasiparticle peak found in DMFT, for example in the series (Sr,Ca)VO_3 [44, 45, 46, 47]. It was thus quite reasonable, to try to describe such materials within a Hubbard model [48, 49]. However, the explanation of the experiments required an unphysical variation of the value of U across the series.

The explanation for the failure lies in the orbital degrees of freedom neglected in the Hubbard model (16.1) but definitely present in transition metal ions. Thus, a development of quantum impurity solvers for models including orbital degrees of freedom started [50, 51, 52]. At the same time it became clear, that the number of adjustable parameters in a multi-orbital Hubbard model increases dramatically with the degrees of freedom. In view of the restricted sets of experiments that one can describe within the DMFT, the idea of material specific calculations with this method actually appears rather ridiculous.

The idea which solved that problem was to use the density functional theory (DFT) [53, 54] to generate the dispersion relation $\epsilon_{\boldsymbol{k}}^{mm'}$ entering the multi-orbital Hubbard model [55, 56]. Moreover, within the so-called constrained DFT [57] even a calculation of Coulomb parameters is possible. Thus equipped, a material-specific many-body theory for transition metal oxides and even lanthanides became possible, nowadays called LDA+DMFT [58, 59, 60, 61]. The scheme basically works as follows [58, 61]:

- For a given material, calculate the band structure using DFT with local density approximation [54].
- Identify the states where local correlations are important and downfold the bandstructure to these states to obtain a Hamilton matrix $\mathbf{H}(\boldsymbol{k})$ describing the dispersion of these states. If necessary, include other states overlapping with the correlated orbitals (for example oxygen $2p$ for transition metal oxides).

– From a constrained DFT calculation, obtain the Coulomb parameters for the correlated orbitals.
– Perform a DMFT calculations using the expression

$$\mathbf{G}_{ii,\sigma}(z) = \frac{1}{N}\sum_{\boldsymbol{k}} \frac{1}{z + \mu - \mathbf{H}(\boldsymbol{k}) - \mathbf{\Sigma}_\sigma(z)} \tag{16.36}$$

for the local Green function, which now can be a matrix in the orbital indices taken into account. Note that the self-energy can be a matrix, too.
– If desired, use the result of the DMFT to modify the potential entering the DFT and repeat from the first step until self-consistency is achieved [56].

As an example for the results obtained in such a parameter-free calculation I present the DOS for (Sr,Ca)VO_3 obtained with the LDA+DMFT scheme compared to photoemission experiments [62] in Fig. 16.9. Apparently, both the position of the structures and the weight are obtained with rather good accuracy. From these calculations one can now infer that the structures seen are indeed the lower Hubbard band originating from the $3d$ levels, here situated at about -2 eV, and a quasiparticle peak describing the coherent states in the system.

This example shows that the DMFT is indeed a rather powerful tool to study 3D materials where local correlations dominate the physical properties. There is, however, not a simple rule of thumb which can tell us when this approach is indeed applicable and when correlations beyond the DMFT may become important. Even in seemingly rather simple systems non-local correlations can be important and modify the dominant effects of the local interactions in a subtle way [63].

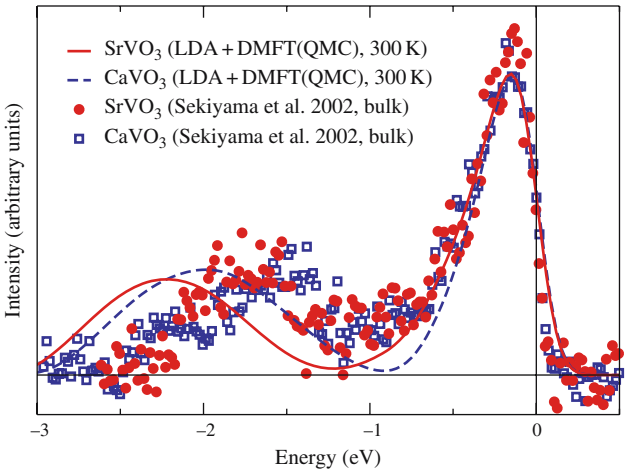

Fig. 16.9. DOS for (Sr,Ca)VO_3 obtained from a parameter free LDA+DMFT calculation (*full lines*) compared to results from photoemission experiments (*symbols*). Taken from [62]

16.3 Extending the DMFT: Effective Cluster Theories

16.3.1 Questions Beyond the DMFT

The DMFT has turned out to be a rather successful theory to describe properties of strongly correlated electron systems in three dimensions sufficiently far away from e.g. magnetic phase transitions. Its strength lies in the fact that it correctly includes the local dynamics induced by the local two-particle interactions. It is, on the other hand, well-known that in one or two dimensions or in the vicinity of a transition to a state with long-range order the physics is rather dominated by non-local dynamics, e.g. spin waves for materials showing magnetic order. Such features are of course beyond the scope of the DMFT.

As a particular example let us take a look at the qualitative properties of the Hubbard model in $D = 2$ on a square lattice at and close to half filling. As we already know, the model has strong antiferromagnetic correlations for intermediate and strong U, leading to a phase transition to a Néel state at finite T_{N} in $D = 3$. However, in $D = 2$ the theorem by Mermin and Wagner [64] inhibits a true phase transition at finite T, only the ground state may show long-range order. Nevertheless, the non-local spin correlations exist and can become strong at low temperature [6]. In particular, a snapshot of the system will increasingly look like the Néel state, at least in a certain vicinity of a given lattice site.

Such a short-range order in both time and space can have profound effects for example on the photoemission spectrum. In a true Néel ordered state the broken translational symmetry leads to a reduced Brillouin zone and hence to a folding back of the bandstructure, as depicted in Fig. 16.10(a). At the boundary of this so-called magnetic Brillouin zone, a crossing of the dispersions occurs, which will be split by interactions and leads to the gap in the DOS and the insulating behavior of the Néel antiferromagnet. When we suppress the long-range order but still allow for short-range correlations, the behavior in Fig. 16.10(b) may occur. There is no true broken translational symmetry, hence the actual dispersion will not change. However, the

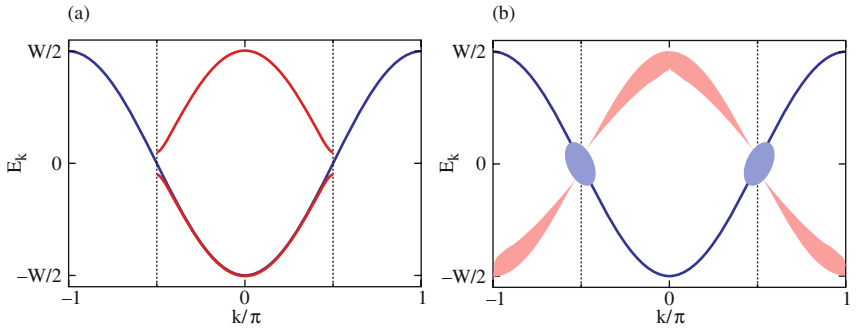

Fig. 16.10. Sketch of the effect of long-range Néel order (**a**) vs. strong short-ranged correlations (**b**) on the single-particle properties of the Hubbard model in $D = 2$

system "feels" the ordered state on certain time and length scales, which leads to broadened structures at the position of the back-folded bands (shadow bands) in the spectral function [65, 66]. Furthermore, the tendency to form a gap at the crossing points at the boundary of the magnetic Brillouin zone can lead to a suppression of spectral weight at these points (pseudo-gaps) [65].

The paradigm for such a behavior surely are the high-T_{C} superconductors, but other low-dimensional materials show similar features, too.

16.3.2 From the Impurity to Clusters

Let us in the beginning state the minimum requirements, that a theory extending the DMFT to include non-local correlation should fulfill: It should

- work in thermodynamic limit,
- treat local dynamics exactly,
- include short-ranged dynamical fluctuations in a systematic and possibly non-perturbative way,
- be complementarity to finite-system calculations
- and of course remain computationally manageable.

It is of course tempting, to try and start from the DMFT as an approximation that already properly includes local dynamics and add the non-local physics somehow. Since the DMFT becomes exact in the limit $D \to \infty$, an expansion in powers of $1/D$ may seem appropriate [67]. However, while such approaches work well for wave functions, their extension to the DMFT suffer from so-called self-avoiding random walk problems, and no proper resummation has been successful yet.

A more pragmatic approach tries to add the non-local fluctuations by hand [68, 69], but here the problem of possible overcounting of processes arises. Moreover, the type of fluctuations included is strongly biased and the way one includes them relies on convergence of the perturbation series.

In yet another idea one extends the DMFT by including two-particle fluctuations locally [70]. In this way, one can indeed observe effects like pseudo-gap formation in the large-U Hubbard model [71], but cannot obtain any $\boldsymbol{k}$-dependence in the spectral function, because the renormalizations are still purely local.

The most successful compromise that fulfills all of the previously stated requirements is based on the concept of clusters. There, the basic idea is to replace the impurity of the DMFT by a small cluster embedded in a medium representing the remaining infinite lattice. In this way, one tries to combine the advantages of finite-system calculations, i.e. the proper treatment of local and at least short-ranged correlations, with the properties of the DMFT, viz the introduction of the thermodynamic limit via the Weiss field. The schematic representation of this approach is shown in Fig. 16.11. This idea is not new, but has been tried in the context of disordered systems before [72], and also in various ways for correlated electron models [24]. A rather successful implementation is the cluster perturbation theory, discussed in Chap. 19. A recent review discussing these previous attempts and their problems is given in [24].

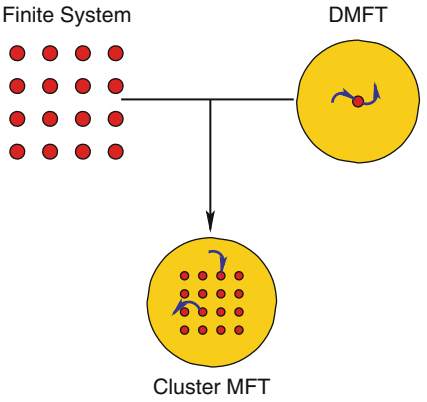

Fig. 16.11. Schematic picture of the idea of a cluster based MFT

16.3.3 Implementing the Algorithm

The implementation of the concept of a cluster MFT is straightforward and will be discussed here using the so-called DCA [24] as example. The other methods basically follow the same strategy, but differ in the details.

The DCA is an extension of the DMFT in $\boldsymbol{k}$-space. Starting from the observation that for short-ranged fluctuations one expects that $\boldsymbol{k}$-dependencies of certain quantities like the single-particle self-energy will be weak, one coarse-grains their $\boldsymbol{k}$-dependence by introducing a suitable set of N_c momenta $\boldsymbol{K}$ in the first Brillouin zone (see Fig. 16.12 with $N_c = 4$ as example). The $\boldsymbol{k}$-dependence of the single-particle self-energy $\Sigma_\sigma(\boldsymbol{k}, z)$ is then approximated according to $\Sigma_\sigma(\boldsymbol{k}, z) \approx \Sigma_\sigma(\boldsymbol{K}, z)$. This means, that one effectively reduces the resolution in real space to length scales $\Delta R \sim \pi/\Delta K$, where ΔK is a measure of the difference of individual

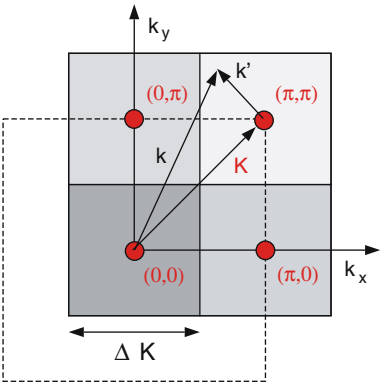

Fig. 16.12. Tiling the first Brillouin zone in the DCA

$\boldsymbol{K}$-vectors in the coarse-grained Brillouin zone. Consequently, we can expect to treat non-local correlations up to this length scale correctly.

The next step now is to integrate out the remaining $\boldsymbol{k}$-vectors in the sectors around each $\boldsymbol{K}$-point. If we do this for the single-particle Green function, we obtain a quantity

$$\bar{G}_\sigma(\boldsymbol{K}, z) := \frac{N_c}{N} \sum_{\boldsymbol{k}'} \frac{1}{z + \mu - \epsilon_{\boldsymbol{K}+\boldsymbol{k}'} - \Sigma_\sigma(\boldsymbol{K}, z)} \tag{16.37}$$

we will call the effective cluster Green function. Obviously, the quantity $\bar{G}_\sigma(\boldsymbol{K}, z)$ describes an effective periodic cluster model. The procedure now follows precisely the ideas of the DMFT. Switching off the interaction in the effective cluster leads to an effective non-interacting system described by a Green function

$$\bar{\mathcal{G}}_\sigma(\boldsymbol{K}, z) = \frac{1}{\bar{G}_\sigma(\boldsymbol{K}, z)^{-1} + \Sigma_\sigma(\boldsymbol{K}, z)} \tag{16.38}$$

and a self-consistency loop depicted in Fig. 16.13.

As in the DMFT, the problematic step is the last box, i.e. the solution of the effective quantum cluster problem. Note that although we started the construction from a cluster, the presence of the energy-dependent medium $\bar{\mathcal{G}}_\sigma(\boldsymbol{K}, z)$ renders this problem again a very complicated many-body problem, just like the effective quantum impurity problem in the DMFT. However, the situation here is even worse, because the dynamical degrees of freedom represented by this medium mean that

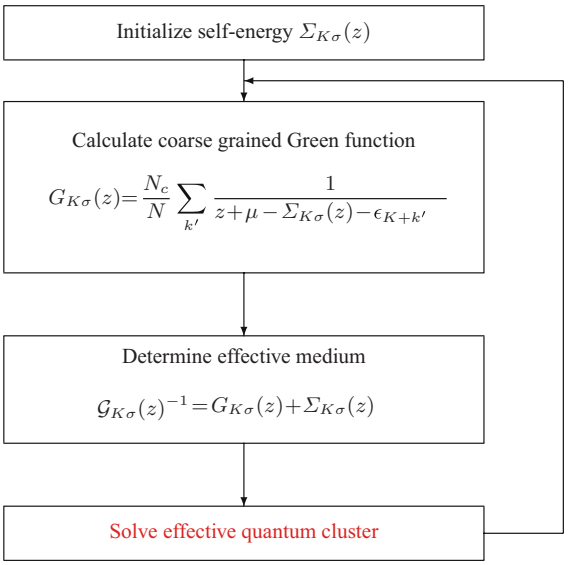

Fig. 16.13. Flow-diagram of the algorithm for the DCA

even for clusters as small as $N_c = 4$, the effective system to solve has infinitely many degrees of freedom. For example the NRG, which is so successful for the Hubbard model in the DMFT, will suffer from a huge increase of the Hilbert space (4^{N_c}) in each step, which makes the method useless. Up to now the only reasonable technique is quantum Monte Carlo (QMC), and most of the results presented in the next section will be based on QMC simulations.

Before we move to the presentation of some results for the Hubbard model, let me make some general comments on the method. First, while the concept of a cluster MFT seems to be a natural extension of the DMFT, it lacks a similar justification by an exact limit. The best one can do is view the cluster MFT as interpolation scheme between the DMFT and the real lattice, systematically including longer ranged correlations. Moreover, the use of a finite cluster introduces the problem of boundary conditions (BC). In a real space implementation [73] one has to use open BC and thus has broken translational invariance. As a consequence, $\boldsymbol{k}$ is not a good quantum number any more and one has to work out averaging procedures to recover the desired diagonality in $\boldsymbol{k}$-space. The DCA implements periodic BC, but introduces patches in the Brillouin zone, where $\Sigma_\sigma(\boldsymbol{K}, z)$ is constant. As result, one obtains a histogram of self-energy values and must use a fitting procedure to recover a smooth function $\Sigma_\sigma(\boldsymbol{k}, z)$, if desired.

Another potential problem can be causality [72]. In early attempts to set up cluster approaches, one typically ran into the problem that spectral functions could become negative. It has been shown, however, that the different implementations of the cluster MFT are manifestly causal [24].

Last but not least one may wonder how one can implement non-local two-particle interactions in this scheme, for example nearest-neighbor Coulomb interaction or the exchange interaction in models like the t-J model. In the DMFT, these interactions reduce to their mean-field description [74]. For cluster mean-field theories, they should in fact be treated similarly to the single-particle hopping. One then is faced with the requirement, to not only solve for dynamic single-particle properties in the presence of the effective bath, but also set up a similar scheme for the two-particle quantities of the effective cluster [24]. In this respect the cluster MFT acquire a structure similar to the so-called EDMT proposed by Q. Si et al. [70].

16.3.4 Results for the Hubbard Model

In the following I present some selected results obtained with the DCA for the Hubbard model in $D = 2$ on a square lattice. If not mentioned otherwise, we will again use the nearest-neighbor hopping (16.15). A much wider overview can be found in the review [24].

The first obvious question to ask is how the cluster MFT will modify the single-particle properties of the Hubbard model. As mentioned, the Mermin-Wagner theorem states that no long-range magnetic order can occur, but from the discussion in the beginning of this chapter we expect at least the presence of strong non-local spin fluctuations which should lead to precursors of the ordering at $T = 0$ in the physical quantities. In Fig. 16.14 the results of calculations for half filling and $U = W/2$ with

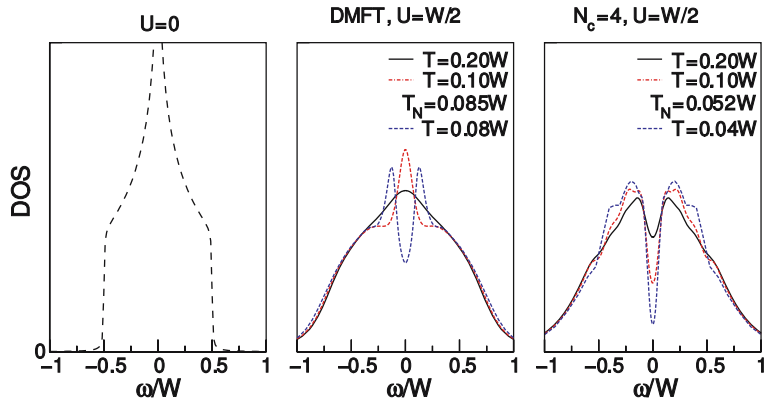

Fig. 16.14. DOS for the $2D$ Hubbard model at half filling and $U = W/2$ for different temperature using the DMFT (**middle panel**) and the DCA with $N_c = 4$ (**right panel**). The left panel shows the bare DOS at $U = 0$ for comparison. Figure taken from [75]

the DMFT (middle panel) and the DCA with a cluster size of $N_c = 4$ (right panel) for different temperatures are shown. For comparison the bare DOS is included in the left panel. In the DMFT, one obtains a phase transition into the Néel state at some $T_\mathrm{N} > 0$. For $T > T_\mathrm{N}$, the DOS shows the ubiquitous three-peak structure, while for $T < T_\mathrm{N}$ a gap appears in the DOS. No precursor of the transition can be seen. The DCA, on the other hand, already shows a pronounced pseudo-gap even at elevated temperatures, which becomes deeper with decreasing temperatures. This reflects the expected presence of spin fluctuations. Since the DCA still represents a MFT, a phase transition will eventually occur here, too. However, the corresponding transition temperature is reduced from its DMFT value and the DOS seemingly varies smoothly from $T > T_\mathrm{N}$ to $T < T_\mathrm{N}$ here.

The influence of spin fluctuations close to half filling can also be seen in the spectral functions $A(\boldsymbol{k}, \omega) = -\operatorname{Im} mG(\boldsymbol{k}, \omega + i0^+)/\pi$, which are plotted along high-symmetry directions of the first Brillouin zone of the square lattice (see Fig. 16.16) in Fig. 16.15. The calculations were done with $N_c = 16$ at a temperature $T = W/30$ at $U = W$ using a Hirsch-Fye QMC algorithm and maximum entropy to obtain the real-frequency spectra from the QMC imaginary time date [24, 77]. In the calculation an additional next-nearest neighbor hopping $t' = 0.05\,W$ was included. For $\langle n \rangle = 0.8$ (left panel of Fig. 16.15) nice quasiparticles along the non-interacting Fermi surface (base-line in the spectra) can be seen and the imaginary part of the self-energy (plot in the left corner of the panel) has a nice parabolic extremum at $\omega = 0$ and is basically $\boldsymbol{k}$-independent. Thus, in this parameter regime the DMFT can be a reliable approximation, at least as far as single-particle properties in the paramagnetic phase are concerned. For $\langle n \rangle = 0.95$ (right panel in Fig. 16.15), on the other hand, quasiparticles are found along the diagonal of the Brillouin zone (cold spot), while the structures are strongly overdamped in the region $\boldsymbol{k} \approx (0, \pi)$ (hot spot). The notion hot spot comes from the observation, that in this region the

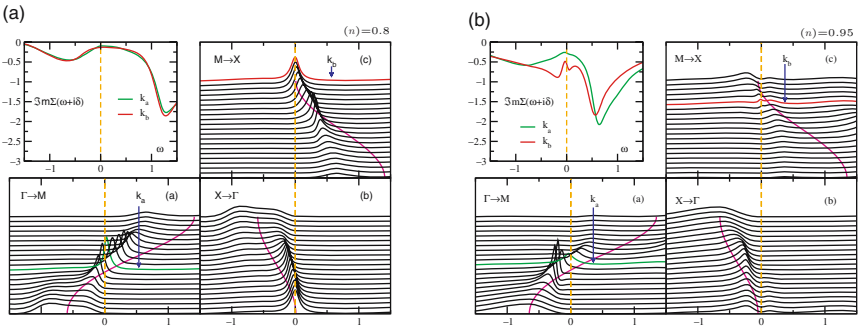

Fig. 16.15. Spectral functions along high-symmetry directions of the first Brillouin zone of the square lattice (see Fig. 16.16) obtained from a DCA calculation with $N_c = 16$ for different fillings $\langle n \rangle = 0.8$ (**left panel**) and $\langle n \rangle = 0.95$ (**right panel**). The figures in the left corners show the imaginary part of the self-energy at special $\boldsymbol{k}$-points indicated by the arrows in the spectra. The model parameters are $U = W$ and $T = W/30$. Figure taken from [76]

Fermi surface can be connected with the reciprocal lattice vector $\boldsymbol{Q}$ describing the antiferromagnetic ordering (see Fig. 16.16) (nesting). Obviously, these $\boldsymbol{k}$-points will be particularly susceptible to spin fluctuations and acquire additional damping due to the coupling to those modes.

Finally, one may wonder what the DCA can do for 3D systems. As example, I show results of a calculation of the Néel temperature for the 3D Hubbard model at half filling in Fig. 16.17. The figure includes several curves: The one labelled "Weiss" is obtained from a Weiss mean-field treatment of the antiferromagnetic Heisenberg model with an exchange coupling $J \sim t^2/U$ according to (16.3). The one called "Heisenberg" represents a full calculation for the 3D Heisenberg model with this exchange coupling, "SOPT" denotes a second-order perturbation theory calculation for the Hubbard model, "Staudt" recent QMC results [79] and finally "DMFT" and "DCA" the values for T_N obtained from DMFT and DCA respectively. Obviously, the DCA results in a substantial reduction of T_N as compared to the DMFT, leading to the correct values for all U. As expected, the DMFT overestimates T_N as usual for a mean-field theory, but, as we already know, is otherwise consistent with the anticipated behavior at both small and large U on the mean-field level.

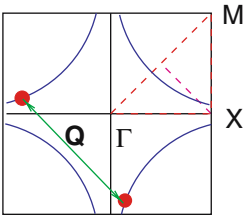

Fig. 16.16. First Brillouin zone of the square lattice

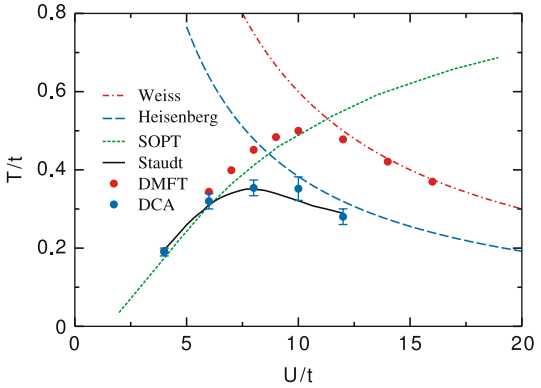

Fig. 16.17. Néel temperature as function of U for the 3D Hubbard model at half filling. For the different curves see text. Taken from [78]

Note that for the QMC results and the DCA a finite size scaling has been performed, where for the DCA lattices up to 32 sites were included, i.e. substantially smaller that in [79].

16.4 Conclusions

Starting from the Weiss mean-field theory for the Heisenberg model, we have developed a proper mean-field theory for correlated fermionic lattice models with local interactions. In contrast to the mean-field theory for the Heisenberg model, the fundamental quantity in this so-called dynamical mean-field theory is the single-particle Green function, and the effective local problem turned out to be a quantum-impurity model. Quantum impurity models are notoriously hard to solve, even with advanced computational techniques. As a special example, we discussed the numerical renormalization group approach in some detail.

As we have seen, the dynamical mean-field theory allows to calculate a variety of static and dynamic properties for correlated lattice models like the Hubbard model and its relatives. In contrast to the Hartree-Fock treatment, dynamical renormalizations lead to non-trivial phenomena like a Fermi liquid with strongly enhanced Fermi liquid parameters, a paramagnetic metal-insulator transition and magnetic properties that correctly describe the crossover from weak-coupling Slater antiferromagnetism to Heisenberg physics and Nagaoka ferromagnetism as $U \to \infty$.

In combination with density functional theory, which allows to determine model parameters for a given material ab initio, a particularly interesting novel approach to a parameter-free and material-specific calculation of properties of correlated materials arises. Several applications have demonstrated the power of this method, which can even lead to a quantitative agreement between theory and experiment.

Thus, is the DMFT an all-in-one tool, suitable for every purpose? Definitely not. We also learned that we have to pay a price for the gain: The DMFT completely

neglects *non-local* fluctuations. This means, for example, that it does not care for the dimensionality of the system and will in particular lead to phase transitions even in nominally one-dimensional problems. Furthermore, even in three dimensions one cannot realize ordered states with non-local order parameters – e.g. d-wave superconductivity. Thus, for low-dimensional system or in the vicinity of phase transitions, the DMFT surely is not a good approach.

These deficiencies can be cured at least in part by extending the notion of *local* to also include clusters in addition to single lattice sites. One then arrives at extensions of the DMFT like the cluster dynamical mean-field theory or the dynamical cluster approximation. These theories allow to incorporate at least spatially short-ranged fluctuations into the calculations. We have learned that these extensions indeed lead to new phenomena, like formation of pseudo-gaps in the one-particle spectra and the appearance of new ordered phases with non-local order parameters. Cluster theories also lead to further renormalizations of transition temperatures or, with large enough clusters, lead to a suppression of phase transitions in low-dimensional systems, in accordance with e.g. the Mermin-Wagner theorem.

Again one has to pay a price for this gain, namely a tremendously increased computational effort. For this reason, calculations are up to now possible only for comparatively high temperatures and only moderate values for the interaction parameters. For the same reason, while the DMFT can also be applied to realistic materials with additional orbital degrees of freedom, cluster mean-field extensions are presently restricted to single-orbital models. Also, questions concerning critical properties of phase transitions are out of reach.

Another phenomenon frequently occurring in correlated electron systems, which cannot be handled by both theories, are quantum phase transitions. This class of phenomena typically involves long-ranged two-particle fluctuations and very low temperatures, which are of course beyond the scope of any computational resource presently available.

The roadmap for further developments and investigations is thus obvious. We need more efficient algorithms to calculate dynamical properties of complex quantum impurity systems, preferably at low temperatures and $T = 0$. First steps into this direction have already been taken through the development of new Monte Carlo algorithms [80, 81] which show much better performance than the conventional Hirsch-Fye algorithm and are also sign-problem free [82].

With more efficient algorithms also new possibilities for studies of properties of correlated electron systems arise: Studies of f-electron systems (heavy Fermions) with DFT+DMFT or even DFT+cluster mean-field theories; low-temperature properties of one- or two-dimensional correlated electron systems with large interaction parameter; critical properties and properties in the vicinity of quantum phase transitions.

This collection of examples shows that, although the DMFT and its cluster extensions are already well established, the list of possible applications and improvements is large and entering into the field by no means without possible reward.

References

1. J. Hubbard, Proc. Roy. Soc. London A **276**, 238 (1963) 473
2. J. Kanamori, Prog. Theor. Phys. **30**, 275 (1963) 473
3. M.C. Gutzwiller, Phys. Rev. Lett. **10**, 159 (1963) 473
4. P. Fulde, *Electron Correlations in Molecules and Solids*. Springer Series in Solid-State Sciences (Springer Verlag, Berlin/Heidelberg/New York, 1991) 474
5. Y. Nagaoka, Phys. Rev. **147**, 392 (1966) 474, 489
6. E. Dagotto, Rev. Mod. Phys. **66**, 763 (1994) 474, 492
7. N. Grewe, H. Keiter, Phys. Rev. B **24**, 4420 (1981) 474
8. N.E. Bickers, Rev. Mod. Phys. **59**, 845 (1987) 474
9. M. Imada, A. Fujimori, Y. Tokura, Rev. Mod. Phys. **70**, 1039 (1998) 475, 490
10. C. Itzykson, J.M. Drouffe, *Statistical Field Theory Vol. I & II* (Cambridge University Press, Cambridge, 1989) 476, 477
11. J. Negele, H. Orland, *Quantum Many-Particle Physics* (Addison-Wesley, 1988) 477, 478, 479, 480, 487
12. W. Metzner, D. Vollhardt, Phys. Rev. Lett. **62**, 324 (1989) 478, 479
13. H. Schweitzer, G. Czycholl, Z. Phys. B **77**, 327 (1990) 480
14. H. Schweitzer, G. Czycholl, Phys. Rev. Lett. **67**, 3724 (1991) 480
15. B. Menge, E. Müller-Hartmann, Z. Phys. B **82**, 237 (1991) 480
16. P.G.J. van Dongen, Phys. Rev. Lett. **67**, 757 (1991) 480, 487
17. P.G.J. van Dongen, Phys. Rev. B **50**, 14016 (1994) 480
18. P.G.J. van Dongen, Phys. Rev. B **54**, 1584 (1996) 480, 489
19. U.B. und C. Mielsch, Z. Phys. B **82**, 37 (1991) 480
20. M. Jarrell, Phys. Rev. Lett. **69**, 168 (1992) 480, 486
21. A. Georges, G. Kotliar, W. Krauth, M.J. Rozenberg, Rev. Mod. Phys. **68**, 13 (1996) 480, 483, 485, 486,
22. A.C. Hewson, *The Kondo Problem to Heavy Fermions*. Cambridge Studies in Magnetism (Cambridge University Press, Cambridge, 1993) 481, 482, 483
23. P.W. Anderson, Phys. Rev. **124**, 41 (1961) 481
24. T.A. Maier, M. Jarrell, T. Pruschke, M. Hettler, Rev. Mod. Phys. **77**, 1027 (2005) 483, 485, 493, 494, 49
25. R. Blankenbecler, D.J. Scalapino, R.L. Sugar, Phys. Rev. D **24**, 2278 (1981) 483
26. M. Feldbacher, K. Held, F. Asaad, Phys. Rev. Lett. **93**, 136405 (2004) 483
27. K.G. Wilson, Rev. Mod. Phys. **47**, 773 (1975) 483
28. R. Bulla, T. Costi, T. Pruschke, (2007). URL `http://arxiv.org/abs/cond-mat/0701105`. Preprint 483
29. H.R. Krishnamurthy, J.W. Wilkins, K.G. Wilson, Phys. Rev. B **21**, 1003 (1980) 483
30. H.R. Krishnamurthy, J.W. Wilkins, K.G. Wilson, Phys. Rev. B **21**, 1044 (1980) 483
31. S. Nishimoto, E. Jeckelmann, J. Phys.: Condens. Matter **16**, 613 (2004) 484
32. S. Nishimoto, T. Pruschke, R.M. Noack, J. Phys.: Condens. Matter **18**, 981 (2006) 484
33. C. Raas, G.S. Uhrig, F.B. Anders, Phys. Rev. B **69**, R041102 (2004) 484
34. T. Pruschke, Prog. Theor. Phys. Suppl. **160**, 274 (2005) 485, 487, 489
35. T. Pruschke, M. Jarrell, J.K. Freericks, Adv. in Phys. **44**, 187 (1995) 485, 490
36. R. Bulla, T.A. Costi, D. Vollhardt, Phys. Rev. B **64**, 045103 (2001) 486, 487
37. G. Moeller, Q. Si, G. Kotliar, M. Rozenberg, D.S. Fisher, Phys. Rev. Lett. **74**, 2082 (1995) 486
38. G. Kotliar, E. Lange, , M.J. Rozenberg, Phys. Rev. Lett. **84**, 5180 (2000) 486
39. R. Bulla, Phys. Rev. Lett. **83**, 136 (1999) 486
40. N.H. Tong, S.Q. Shen, F.C. Pu, Phys. Rev. B **64**, 235109 (2001) 487
41. M. Jarrell, T. Pruschke, Z. Phys. B **90**, 187 (1993) 487
42. R. Zitzler, T. Pruschke, R. Bulla, Eur. Phys. J. B **27**, 473 (2002) 487, 489

43. T. Pruschke, R. Zitzler, J. Phys.: Condens. Matter **15**, 7867 (2003) 489
44. Y. Aiura, F. Iga, Y. Nishihara, H. Ohnuki, H. Kato, Phys. Rev. B **47**, 6732 (1993) 490
45. K. Morikawa, T. Mizokawa, K. Kobayashi, A. Fujimori, H. Eisaki, S. Uchida, F. Iga, Y. Nishihara, Phys. Rev. B **52**, 13711 (1995) 490
46. K. Maiti, D.D. Sarma, M.J. Rozenberg, I.H. Inoue, H. Makino, O. Goto, M. Pedio, R. Cimino, Europhys. Lett. **55**, 246 (2001) 490
47. I.H. Inoue, C. Bergemann, I. Hase, S.R. Julian, Phys. Rev. Lett. **88**, 236403 (2002) 490
48. M.J. Rozenberg, G. Kotliar, H. Kajueter, G.A. Thomas, D.H. Rapkine, J.M. Honig, P. Metcalf, Phys. Rev. Lett. **75**, 105 (1995) 490
49. M.J. Rozenberg, I.H. Inoue, H. Makino, F. Iga, Y. Nishihara, Phys. Rev. Lett. **76**, 4781 (1996) 490
50. M.J. Rozenberg, Phys. Rev. B **55**, R4855 (1997) 490
51. J.E. Han, M. Jarrell, D.L. Cox, Phys. Rev. B **58**, 4199 (1998) 490
52. K. Held, D. Vollhardt, Eur. Phys. J. B **5**, 473 (1998) 490
53. O.K. Andersen, Phys. Rev. B **12**, 3060 (1975) 490
54. R.O. Jones, O. Gunnarsson, Rev. Mod. Phys. **61**, 689 (1989) 490
55. V.I. Anisimov, A.I. Poteryaev, M.A. Korotin, A.O. Anokhin, G. Kotliar, J. Phys.: Condens. Matter **9**, 7359 (1997) 490
56. V.I. Anisimov, D.E. Kondakov, A.V. Kozhevnikov, I.A. Nekrasov, Z.V. Pchelkina, J.W. Allen, S.K. Mo, H.D. Kim, P. Metcalf, S. Suga, A. Sekiyama, G. Keller, I. Leonov, X. Ren, D. Vollhardt, Phys. Rev. B **71**, 125119 (2005) 490, 491
57. V.I. Anisimov, O. Gunnarsson, Phys. Rev. B **43**, 7570 (1991) 490
58. K. Held, I.A. Nekrasov, G. Keller, V. Eyert, N. Blümer, A.K. McMahan, R.T. Scalettar, T. Pruschke, V.I. Anisimov, D. Vollhardt, in *Quantum Simulations of Complex Many-Body Systems: From Theory to Algorithms*, *NIC Series*, vol. 10, ed. by J. Grotendorst, D. Marks, A. Muramatsu (2002), *NIC Series*, vol. 10, pp. 175–209 490
59. K. Held, I.A. Nekrasov, N. Blümer, V.I. Anisimov, D. Vollhardt, Int. J. Mod. Phys. **15**, 2611 (2001) 490
60. K. Held, I.A. Nekrasov, G. Keller, V. Eyert, N. Blümer, A.K. McMahan, R.T. Scalettar, T. Pruschke, V.I. Anisimov, D. Vollhardt, 490
61. G. Kotliar, S.Y. Savrasov, K. Haule, V.S. Oudovenko, O. Parcollet, C.A. Marianetti, Rev. Mod. Phys. **78**, 865 (2006) 490
62. A. Sekiyama, H. Fujiwara, S. Imada, S. Suga, H. Eisaki, S.I. Uchida, K. Takegahara, H. Harima, Y. Saitoh, I.A. Nekrasov, G. Keller, D.E. Kondakov, A.V. Kozhevnikov, T. Pruschke, K. Held, D. Vollhardt, V.I. Anisimov, Phys. Rev. Lett. **93**, 156402 (2004) 491
63. A.I. Poteryaev, A.I. Lichtenstein, G. Kotliar, Phys. Rev. Lett. **93**, 086401 (2004) 491
64. A. Gelfert, W. Nolting, Journal of Physics: Condensed Matter **13**, R505 (2001) 492
65. A. Kampf, J.R. Schrieffer, Phys. Rev. B **41**, 6399 (1990) 493
66. A.P. Kampf, J.R. Schrieffer, Phys. Rev. B **42**, 7967 (1990) 493
67. F. Gebhard, Phys. Rev. B **41**, 9452 (1990) 493
68. T. Obermeier, T. Pruschke, J. Keller, Physica B **230–232**, 892 (1997) 493
69. M.V. Sadovskii, I.A. Nekrasov, E.Z. Kuchinskii, T. Pruschke, V.I. Anisimov, Phys. Rev. B **72**, 155105 (2005) 493
70. J.L. Smith, Q. Si, Phys. Rev. B **61**, 5184 (2000) 493, 496
71. K. Haule, A. Rosch, J. Kroha, P. Wölfle, Phys. Rev. Lett. **89**, 236402 (2002) 493
72. A. Gonis, *Green Functions for Ordered and Disordered Systems*. Studies in Mathematical Physics (North-Holland, Amsterdam, 1992) 493, 496
73. G. Kotliar, S.Y. Savrasov, G. Pallson, G. Biroli, Phys. Rev. Lett. **87**, 186401 (2001) 496
74. E. Müller-Hartmann, Z. Phys. **B 74**, 507 (1989) 496

75. T. Maier, M. Jarrell, T. Pruschke, J. Keller, Eur. Phys. J. B **13**, 613 (2000) 497
76. T.A. Maier, T. Pruschke, M. Jarrell, Phys. Rev. B **66**, 075102 (2002) 498
77. M. Jarrell, J.E. Gubernatis, Physics Reports **269**, 133 (1996) 497
78. P.R.C. Kent, M. Jarrell, T.A. Maier, T. Pruschke, Phys. Rev. B **72**, 060411 (2005) 499
79. R. Staudt, M. Dzierzawa, A. Muramatsu, Eur. Phys. J. B **17**, 411 (2000) 498, 499
80. A.N. Rubtsov, V.V. Savkin, A.I. Lichtenstein, Phys. Rev. B **72**, 035122 (2005) 500
81. P. Werner, A.J. Millis, Phys. Rev. B **74**, 155107 (2006) 500
82. E. Gull, P. Werner, A.J. Millis, M. Troyer, (2006). URL `http://arxiv.org/abs/cond-mat/0609438`. Preprint 500